

Relationship between Oxidation Level and Optical Properties of Secondary Organic Aerosol

Andrew T. Lambe,^{*,†,‡} Christopher D. Cappa,[§] Paola Massoli,[‡] Timothy B. Onasch,^{†,‡} Sara D. Forestieri,[§] Alexander T. Martin,[†] Molly J. Cummings,[†] David R. Croasdale,[†] William H. Brune,^{||} Douglas R. Worsnop,[‡] and Paul Davidovits[†]

[†]Chemistry Department, Boston College, Chestnut Hill, Massachusetts, United States

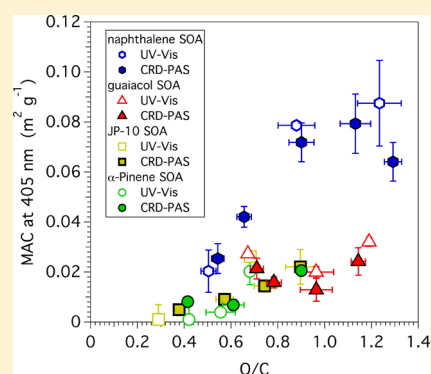
[‡]Aerodyne Research, Inc., Billerica, Massachusetts, United States

[§]Department of Civil and Environmental Engineering, University of California, Davis, California, United States

^{||}Department of Meteorology and Atmospheric Sciences, The Pennsylvania State University, University Park, Pennsylvania, United States

Supporting Information

ABSTRACT: Brown carbon (BrC), which may include secondary organic aerosol (SOA), can be a significant climate-forcing agent via its optical absorption properties. However, the overall contribution of SOA to BrC remains poorly understood. Here, correlations between oxidation level and optical properties of SOA are examined. SOA was generated in a flow reactor in the absence of NO_x by OH oxidation of gas-phase precursors used as surrogates for anthropogenic (naphthalene, tricyclo-[5.2.1.0^{2,6}]decane), biomass burning (guaiacol), and biogenic (α -pinene) emissions. SOA chemical composition was characterized with a time-of-flight aerosol mass spectrometer. SOA mass-specific absorption cross sections (MAC) and refractive indices were calculated from real-time cavity ring-down photoacoustic spectrometry measurements at 405 and 532 nm and from UV-vis spectrometry measurements of methanol extracts of filter-collected particles (300 to 600 nm). At 405 nm, SOA MAC values and imaginary refractive indices increased with increasing oxidation level and decreased with increasing wavelength, leading to negligible absorption at 532 nm. Real refractive indices of SOA decreased with increasing oxidation level. Comparison with literature studies suggests that under typical polluted conditions the effect of NO_x on SOA absorption is small. SOA may contribute significantly to atmospheric BrC, with the magnitude dependent on both precursor type and oxidation level.



1. INTRODUCTION

Atmospheric light-absorbing carbon (LAC) particles, which include black carbon (BC) and brown carbon (BrC) from compounds such as humic-like substances (HULIS) and organic aerosols associated with biomass burning (BBOA),¹ play an important role in global climate change.^{2,3} The optical properties of BC are well-defined and suggest that soot dominates absorption of light at wavelengths above ~ 500 nm.⁴ At lower wavelengths of the solar spectrum (300 to 500 nm), the light absorption by BrC may be substantial.^{5–10} A few modeling studies suggest that BrC contributes 0.1 to 0.25 W m^{-2} to global radiative forcing, compared to ~ 1.1 W m^{-2} of BC.^{11,12} However, the results from such studies rely on having accurate knowledge of the optical properties of BrC, which are not well established and can vary dramatically by source.

Secondary organic aerosols (SOA), which dominate the global OA budget,¹³ also contribute to atmospheric LAC.^{14,15} SOA optical properties have been determined only for a limited subset of source types and atmospheric conditions because of the difficulty of measuring these parameters with high sensitivity and time resolution. In previous laboratory experi-

ments, optical properties of SOA from the following systems have been studied: photooxidation of phenolic precursors,^{16–18} OH oxidation of α -pinene, limonene, and toluene in the presence of NO_x ,^{19–25} and “aged” SOA exposed to NH_3 and NH_4^+ .^{26–29} A large fraction of atmospheric SOA is produced by oxidation of precursors under low- NO_x conditions and downwind of urban locations.^{30,31} Light absorption of SOA formed from OH oxidation of limonene and α -pinene in the absence of NO_x has been observed.³² However, the studies have not systematically or quantitatively characterized optical properties such as mass-specific absorption cross sections (MAC) and complex refractive indices (k), the latter parameter related to the MAC by particle density ($\text{MAC} = 4\pi k/\lambda\rho$). As a result, the parameters governing optical absorption of such SOA, and their influence on global climate forcing, remain poorly understood.

Received: March 7, 2013

Revised: May 18, 2013

Accepted: May 23, 2013

Published: May 23, 2013

In the present work we report on the characterization of MAC values and complex refractive indices of SOA generated in the absence of NO_x by the OH oxidation of four gas-phase precursors selected as surrogates for anthropogenic aromatic (naphthalene), anthropogenic aliphatic (tricyclo[5.2.1.0^{2,6}]-decane), biomass burning (guaiacol), and biogenic (α -pinene) emissions. Oxidation experiments were conducted using a flow reactor³³ that provides OH exposures up to 1.5×10^{12} molecules cm^{-3} s, which corresponds to multiple days of atmospheric oxidation and is approximately ten times higher than exposures attainable with environmental chambers. Additionally, the effect of NO_x on optical properties of α -pinene and naphthalene SOA is examined by comparing our results with previous measurements in which SOA was formed in the presence of NO_x . Finally, the optical properties of several humic and fulvic acid materials, commonly used as laboratory surrogates for ambient HULIS,³⁴ were also measured as proxies for primary BrC and for comparison with the SOA results.

2. EXPERIMENTAL SECTION

2.1. SOA Production. SOA particles were generated in a Potential Aerosol Mass (PAM) flow reactor³⁵ by homogeneous nucleation and condensation following OH oxidation of gas-phase precursors. The average gas-phase species residence time in the PAM reactor was approximately 100 s. The level of oxidation was controlled by the OH concentration in the reactor. Naphthalene vapor was introduced by flowing ultrapure zero air over solid naphthalene placed in a Teflon tube. Guaiacol (heated to 30 °C), tricyclo[5.2.1.0^{2,6}]decane (JP-10), and α -pinene were evaporated from glass bubblers at controlled rates using a carrier gas of ultrapure zero air.

2.2. OH Radical Generation. OH radicals were produced via the reaction $\text{O}(^1\text{D}) + \text{H}_2\text{O} \rightarrow 2\text{OH}$, with $\text{O}(^1\text{D})$ radicals produced from the reaction $\text{O}_3 + h\nu \rightarrow \text{O}_2 + \text{O}(^1\text{D})$. O_3 was generated by irradiating O_2 with a mercury lamp ($\lambda = 185$ nm) outside the PAM reactor. The $\text{O}(^1\text{D})$ radicals were produced by UV photolysis of O_3 inside the PAM reactor using four mercury lamps (BHK Inc.), with peak emission intensity at $\lambda = 254$ nm. These lamps were mounted in Teflon-coated quartz cylindrical sleeves and were continually purged with N_2 . Water vapor was introduced using a heated Nafion membrane humidifier (Perma Pure LLC). The humidifier temperature was set to provide a controlled relative humidity (RH) in the range of 30–40% RH. A carrier gas of 8.5 L/min N_2 and 0.5 L/min O_2 was used.

The OH exposure, which is the product of the OH concentration and the average residence time in the PAM reactor, was determined by measuring the decay of SO_2 due to reaction with OH. The OH concentration was varied by changing the UV light intensity through stepping the lamp voltages between 0 and 110 V. The OH exposures ranged from $(2.2 \pm 1.1) \times 10^{11}$ to $(1.5 \pm 0.2) \times 10^{12}$ molecules cm^{-3} s or approximately 1.5 to 12 days of equivalent atmospheric exposure at a typical OH concentration of 1.5×10^6 molecules cm^{-3} .³⁶ Simple rate calculations suggest that the UV light within the PAM reactor does not significantly affect the SOA oxidation process because upper-bound time scales for UV photolysis of compounds that condense to form SOA are much slower than time scales for gas-phase or condensed-phase OH oxidation (Table S1).

2.3. Particle Monitoring, Collection, and Analysis. A schematic of the experimental setup is shown in Figure S1. Particles exiting the PAM reactor pass through annular

denuders filled with Carulite 200 catalyst (Carus Corp.) and activated charcoal to remove ozone and gas-phase organics. Particle mobility size distributions were measured with a scanning mobility particle sizer (SMPS, TSI 3080). Particle mass spectra and aerodynamic size distributions were measured with an Aerodyne compact time-of-flight aerosol mass spectrometer (c-ToF-AMS)³⁷ and analyzed using high resolution ToF-AMS analysis software.³⁸ The mass spectra yielded hydrogen-to-carbon (H/C) and oxygen-to-carbon (O/C) elemental ratios in the SOA from the measured abundances of the C_xH_y^+ , $\text{C}_x\text{H}_y\text{O}^+$, and $\text{C}_x\text{H}_y\text{O}_2^+$ HR ion groups containing zero, one, and two or more oxygen atoms per ion, respectively. The ions O^+ , OH^+ , H_2O^+ , and CO^+ were included in the $\text{C}_x\text{H}_y\text{O}_2^+$ group because concentrations of these species were calculated from the organic CO_2^+ ion abundance using the recommendations of Aiken et al.³⁹

In one set of experiments, SOA particles were collected onto Teflon filters (47 mm diameter, 0.45 μm pore size) with collection times ranging from 4 to 24 h depending on the SOA concentration. After collection, SOA was extracted from filters via ultrasonication in methanol for 30 min. The SOA extracts were analyzed using a high-resolution UV–vis spectrometer coupled to a deuterium tungsten halogen source (Ocean Optics, Inc.). Typical uncertainties in these measurements were approximately 10%. In addition to the measurements for filter-collected SOA, UV–vis spectra were also measured for Suwannee River fulvic acid, Leonardite humic acid, Elliot Soil humic acid, and Pahokee Peat humic acid (International Humic Substances Society). These humic and fulvic acid standards were dissolved in 0.1 M NaOH for UV–vis analysis.⁴⁰

In a separate set of experiments, particle light extinction and absorption coefficients (b_{ext} , b_{abs} ; Mm^{-1}) were measured with a combined cavity ringdown and photoacoustic spectrometer (CRD-PAS)^{41–45} after drying the aerosol to <30% RH. The CRD measures b_{ext} and the PAS measures b_{abs} at both 405 nm and at 532 nm. The PAS was calibrated using gas-phase O_3 by referencing the observed photoacoustic signal to the corresponding b_{ext} measured with the CRD. The measured detection limits of the PAS instrument for SOA absorption were approximately 0.8 Mm^{-1} at 405 nm and 0.4 Mm^{-1} at 532 nm. Observed b_{abs} values were above the PAS detection limit at 405 nm but below the PAS detection limit at 532 nm. Typical uncertainties were <5% for b_{ext} at 405 and 532 nm and 20% for b_{abs} at 405 nm.

2.3.1. Calculation of SOA Optical Properties. The combined set of SMPS, ToF-AMS, CRD-PAS, and UV/vis measurements yields SOA mobility and aerodynamic size distributions, mass concentrations, b_{ext} , b_{abs} (Mm^{-1}), and MAC ($\text{m}^2 \text{g}^{-1}$) values. The SOA MAC values obtained from UV–vis measurements were calculated using eq 1

$$\text{MAC}_{\text{UV-vis}} = \frac{A}{[\text{SOA}]_e \times L} \quad (1)$$

where A is the measured absorbance, $[\text{SOA}]_e$ is the mass concentration of SOA in the methanol extract, and L is the UV–vis spectrometer path length. SOA MAC values from the PAS were calculated at 405 nm as $\text{MAC}_{\text{PAS}} = b_{\text{abs}}/C_{\text{SOA}}$, where C_{SOA} is the particle mass concentration obtained from the integrated SMPS volume multiplied by the effective density ρ_{eff} .⁴⁶

$$\rho_{\text{eff}} = \rho_0 \times \frac{D_{\text{va}}}{D_{\text{m}}} \quad (2)$$

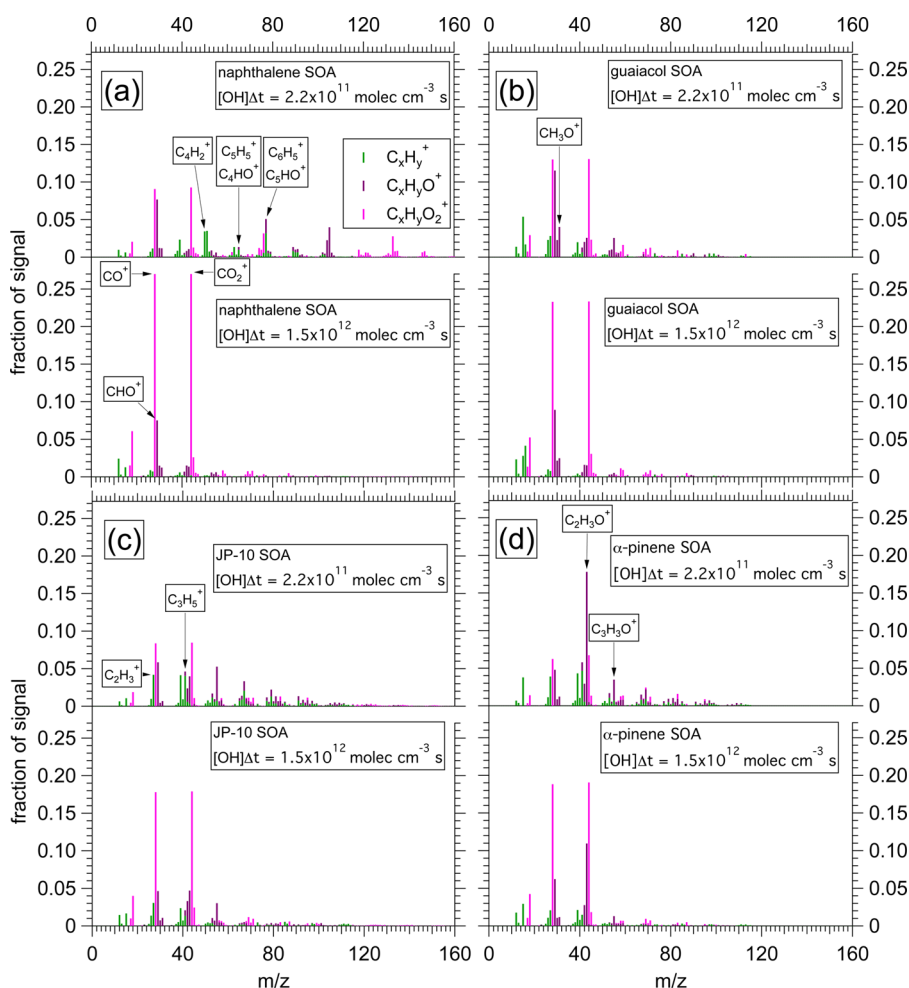


Figure 1. Mass spectra of laboratory SOA generated from OH oxidation of (a) naphthalene, (b) guaiacol, (c) tricyclo[5.2.1.0^{2,6}]decane (JP-10), and (d) α -pinene at OH exposures of 2.2×10^{11} and 1.5×10^{12} molecules cm^{-3} s.

Here $\rho_0 = 1 \text{ g cm}^{-3}$, D_{va} is the vacuum aerodynamic diameter obtained from AMS measurements, and D_m is the volume-weighted mobility diameter obtained from SMPS measurements. The SOA ρ_{eff} ranged from 1.23 to 1.70 g cm^{-3} depending on SOA precursor type and oxidation level (Figures S1 and S2).

Real and imaginary refractive indices of SOA at 405 and 532 nm were determined from minimization of the chi-square between the measured and calculated extinction and absorption, where the calculations utilized spherical particle Mie theory constrained by the measured SMPS size distribution. Mie theory code developed in Bohren and Huffman⁴⁷ was numerically implemented in Igor Pro (Wave-metrics, Inc.). The range of real (n) and imaginary (k) refractive index values considered in the least-squares optimization algorithm were $n = 1.4$ to 1.7 and $k = 0.0001$ to 0.025 .

3. RESULTS AND DISCUSSION

3.1. SOA Mass Spectra, O/C and H/C Ratios. AMS mass spectra of the four SOA types are shown in Figure 1 for low and high OH exposures of 2.2×10^{11} and 1.5×10^{12} molecules cm^{-3} s, respectively. At low OH exposures, the mass spectra depend on the precursor identity, and the observed C_xH_y^+ and $\text{C}_x\text{H}_y\text{O}^+$ ion signals provide an indication of the chemical nature of early-generation oxidation products. All low-OH SOA

spectra exhibit significant intensity at $m/z = 29$ (CHO^+) and $m/z = 43$ ($\text{C}_2\text{H}_3\text{O}^+$), indicative of carbonyl ions. In addition, low-OH AMS spectra of naphthalene and guaiacol SOA have significant intensity at $m/z = 50$ – 51 (C_4H_2^+ , C_4H_3^+), $m/z = 65$ (C_3H_5^+ , C_4HO^+), and $m/z = 76$ – 77 (C_6H_5^+ , C_3HO^+), which are characteristic of aromatic compounds. The guaiacol SOA mass spectrum also has a strong signal at $m/z = 31$ (CH_3O^+) which results from the methoxy group that is present in the precursor. Unlike the aromatic SOA spectra, ions indicative of cycloalkyl fragments (e.g., $m/z = 27$, C_2H_3^+ ; $m/z = 41$, C_3H_5^+ ; $m/z = 55$, $\text{C}_3\text{H}_3\text{O}^+$) are present in JP-10 SOA and α -pinene SOA spectra at significant intensities. For all species, as the OH exposure increases, the most notable change is an increase in signal at $m/z = 44$ (CO_2^+), which is a signature of organic acids,³⁹ and in signals for other $\text{C}_x\text{H}_y\text{O}_2^+$ ions. Correspondingly, the relative abundance of aromatic, cycloalkyl, and carbonyl ions decreases as the AMS signal at $m/z = 44$ increases, suggesting that at high OH exposures the SOA is increasingly dominated by organic acids.

From the AMS spectra, the O/C and the H/C ratios are extracted using high-resolution AMS analysis software. Figure 2 shows a Van Krevelen diagram⁴⁸ (H/C ratio as a function of O/C ratio) for the SOA types studied. The O/C ratio increases with OH exposure for all SOA types, indicating addition of oxygen-containing functional groups. The evolution of the SOA H/C ratio depends on the precursor, but in general it decreases

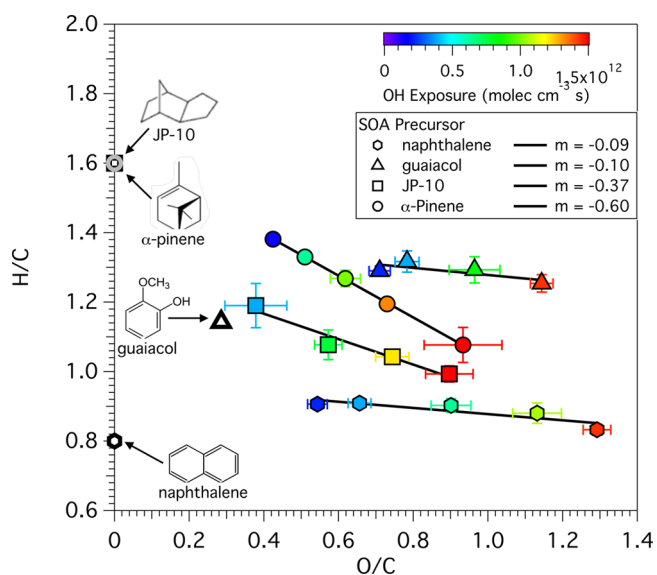


Figure 2. Van Krevelen diagram showing the H/C ratio as a function of the O/C ratio for SOA produced from OH oxidation of naphthalene, guaiacol, JP-10, and α -pinene. Symbols are colored by OH exposure in the PAM reactor. Representative error bars represent $\pm 1\sigma$ in replicate measurements. Open black/gray symbols represent H/C and O/C ratios of SOA precursors.

with OH exposure, indicating hydrogen loss due to formation of C=O bonds. Changes in H/C and O/C ratios of the SOA

are well described by linear fits with $\Delta(\text{H/C})/\Delta(\text{O/C})$ slopes of -0.09 ± 0.03 for naphthalene SOA, -0.10 ± 0.06 for guaiacol SOA, -0.37 ± 0.06 for JP-10 SOA, and -0.60 ± 0.01 for α -pinene SOA. The Van Krevelen slopes of ~ 0 for naphthalene SOA and guaiacol SOA are consistent with initial OH addition to aromatic rings in these systems,^{49,50} which results in a higher H/C ratio than the precursors. The Van Krevelen slopes for α -pinene and JP-10 SOA are consistent with hydrogen abstraction followed by addition of carbonyl and carboxylic acid groups and fragmentation reactions that result in carbon loss from the SOA.^{51,52}

3.2. Mass Absorption Cross Sections (MAC) of SOA.

3.2.1. MAC as a Function of O/C Ratio and Wavelength. The wavelength-dependent absorption of SOA methanol extracts and humic/fulvic acids was measured using UV-vis spectrometry and is shown in Figure 3. Figure 3a–c shows MAC as a function of wavelength (300 to 600 nm) for the four SOA types. Figure 3d shows MAC as a function of wavelength for the fulvic acid and humic acids studied in the present experiments. The fulvic acid and humic acid MAC values span the range of literature values for other types of BrC.

First, we note that the MAC values obtained from the CRD-PAS and the UV-vis measurements agree to within about $\pm 25\%$ at 405 nm (Figure 4). For example, the MAC values of naphthalene SOA at $\text{O/C} \approx 0.5$ were $0.025 \pm 0.006 \text{ m}^2 \text{ g}^{-1}$ and $0.020 \pm 0.008 \text{ m}^2 \text{ g}^{-1}$ from the UV-vis data and CRD-PAS data, respectively. At $\text{O/C} \approx 1.2$, the MAC of naphthalene SOA was measured to be $0.088 \pm 0.017 \text{ m}^2 \text{ g}^{-1}$

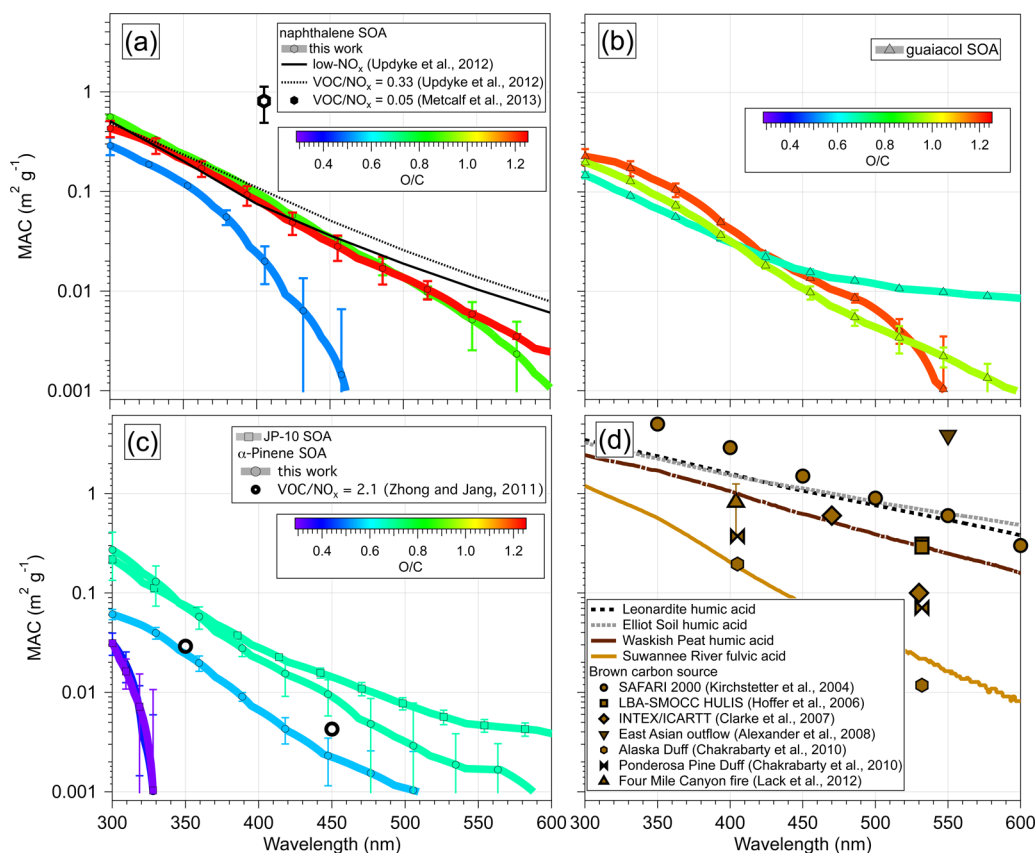


Figure 3. Mass-specific absorption cross sections of (a) naphthalene SOA, (b) guaiacol SOA, (c) α -pinene and JP-10 SOA, and (d) humic/fulvic acids and ambient sources of BrC as a function of wavelength. Measurements were obtained with a UV-vis spectrometer; error bars represent $\pm 1\sigma$ of replicate measurements. Symbols in (a)–(c) are colored by the O/C ratio of the SOA.

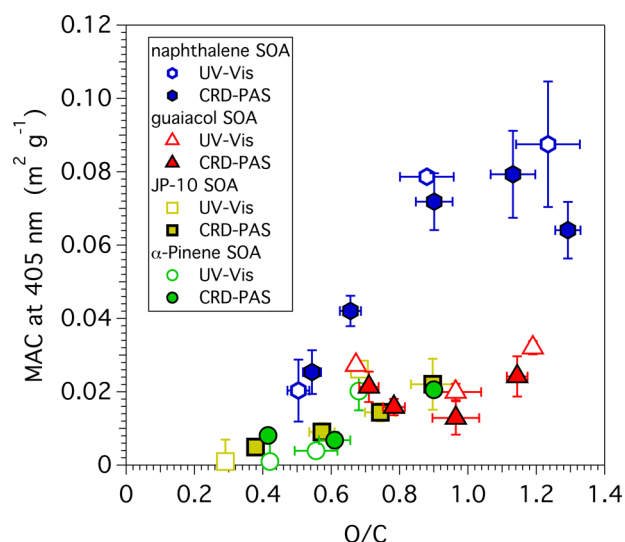


Figure 4. Mass-specific absorption cross sections (MAC) of SOA at $\lambda = 405$ nm as a function of the O/C ratio. Error bars represent $\pm 1\sigma$ of replicate measurements.

from the UV-vis and 0.064 ± 0.008 $\text{m}^2 \text{g}^{-1}$ from the CRD-PAS. Similar agreement was observed for the other SOA types.

Further, the following features are noted in Figure 3. (i) The MAC values of SOA produced from naphthalene, JP-10, and α -pinene increase as a function of the O/C ratio over all wavelengths studied, while the MAC of guaiacol SOA displays a different trend. For guaiacol SOA, the MAC increases with the O/C ratio at $\lambda < 400$ nm, decreases and then increases with an increasing O/C ratio for $\lambda = 400$ to 525 nm, and decreases with an increasing O/C ratio for $\lambda > 525$ nm. (ii) In general, naphthalene and guaiacol SOA have larger MAC values than JP-10 and α -pinene SOA, particularly at the lowest oxidation levels and at $\lambda < 400$ nm. The larger MAC values for naphthalene and guaiacol SOA are probably due to the aromaticity of these two gas-phase precursors, which may in part be preserved in the SOA (Figure 1). (iii) The MAC values of SOA are lower than for other types of BrC (Figure 3d) and for BC.⁴ For example, MAC values at 405 nm range from approximately 0.20 to 4.1 $\text{m}^2 \text{g}^{-1}$ for ambient BBOA and HULIS,^{5,9,53–56} from 0.18 to 1.5 $\text{m}^2 \text{g}^{-1}$ for humic and fulvic acids, and from 0.001 to 0.088 $\text{m}^2 \text{g}^{-1}$ for SOA characterized here. (iv) For all SOA studied here, the MAC decreases monotonically with increasing wavelength (at a given O/C ratio), similar to BBOA.¹⁰ The wavelength dependence of the MAC can be expressed in terms of an absorption Ångstrom exponent (AAE) characterized using eq 3:

$$\frac{\text{MAC}_{\lambda_1}}{\text{MAC}_{\lambda_2}} = \left(\frac{\lambda_1}{\lambda_2} \right)^{-\text{AAE}} \quad (3)$$

There is no systematic correlation between SOA oxidation level and AAE (Table S2).

3.2.2. Suggested Mechanism for SOA Optical Absorption.

Our observations indicate the formation of chromophores in the SOA that absorb light at wavelengths ranging from 300 to 600 nm. The monotonic decrease in MAC as a function of wavelength suggests maximum MAC values occur at $\lambda < 300$ nm. For the SOA types studied, this suggests that their visible light absorption over the solar radiation spectrum is determined by the high-wavelength tail of the absorption spectrum of the

individual compounds (Figure 3). Maximum overlap between the SOA MAC values and solar spectral irradiance distribution occurs at $\lambda \approx 310$ –350 nm.⁵⁷

From the AMS spectra (Figure 1), the Van Krevelen diagram (Figure 2), and optical absorption properties of SOA (Figures 3 and 4), we suggest that the increase in MAC values with oxidative aging is due in part to the increase in carboxylic acid and carbonyl content of the SOA. The increase in abundance of multiple adjacent, oxygen-containing functional groups per molecule increases the level of conjugation in the SOA and extends light absorption toward longer wavelengths. To support this hypothesis, Figure 5 shows UV-vis spectra

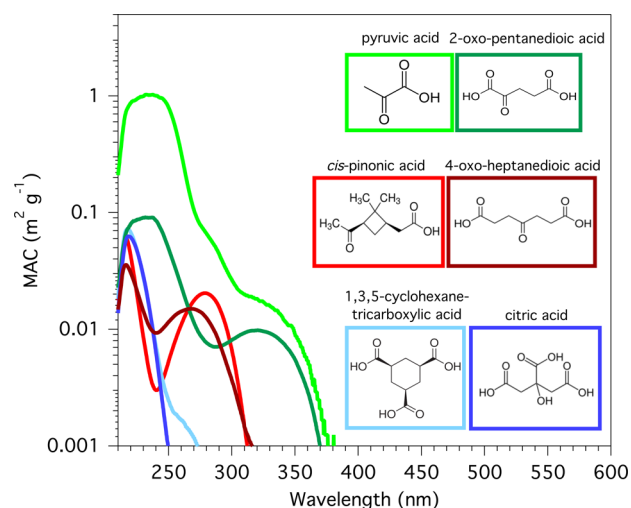


Figure 5. Mass-specific absorption cross sections (MAC) of selected carboxylic acid standards obtained from UV/vis spectrometer measurements.

obtained for several organic acids of known composition: citric acid, 1,3,5-cyclohexanetricarboxylic acid, *cis*-pinonic acid, 4-oxoheptanedioic acid, 2-oxopentanedioic acid, and pyruvic acid. Only 2-oxopentanedioic acid and pyruvic acid, both of which contain adjacent carboxylic acid and carbonyl functional groups (i.e., in α , β -positions), absorb visible light above 350 nm, although none exhibit significant absorption above 400 nm. This suggests either more extensive conjugation in SOA relative to these individual compounds or the formation of additional chromophores that are not identified by the AMS spectra.

Under zero- NO_x conditions, for the nonaromatic precursors, organic peroxides can be formed with significant yields^{24,50,58–60} and may increase visible absorption in conjunction with other chromophores.^{61,62} While organic peroxides can be detected in their dehydrated form with the AMS, supplementary measurement techniques are required for unambiguous confirmation.^{63,64} Thus, their influence may be underestimated in the AMS spectra and Van Krevelen diagrams shown in Figures 1 and 2. Oxidation of nonaromatic precursors can lead to small yields of aromatic products (e.g., *p*-cymene from α -pinene ozonolysis/photooxidation⁶⁵) and may represent an additional mechanism leading to chromophore formation. Condensed phase reactions can also lead to oligomer formation, which may further affect the optical properties of the OA.

For the aromatic precursors, light-absorbing conjugated double bonds are retained in some oxidation products, as suggested by Figure 1a and b and previous studies.^{50,66}

Conjugated double bonds can also extend absorption out toward longer wavelengths in the UV–vis region. These differences in functional groups formed for the aromatic vs nonaromatic SOA precursors may explain differences in the MAC vs O/C ratio slopes between these systems (Figure 4). Macromolecular humic and fulvic acids, which contain conjugated double bonds and significant carboxylic acid and carbonyl content,^{67,68} may therefore represent upper limits for SOA MAC values (Figure 3d).

3.2.3. The Effect of NO_x on MAC of Naphthalene and α -Pinene SOA. Previous studies have shown that addition of NO_x can increase the refractive indices and/or MAC of SOA relative to zero-NO_x conditions.^{20–22,26} Figure 3a shows literature MAC measurements obtained for naphthalene SOA in the presence of NO_x.^{26,69} At 405 nm, Updyke et al.²⁶ measured MAC = 0.10 m² g⁻¹ in the presence of NO_x (VOC/NO_x = 0.33) compared to 0.07 m² g⁻¹ in the absence of NO_x (O/C ratio not reported). This value falls in the range of MAC = 0.020 to 0.088 m² g⁻¹ measured in this work, over O/C ratios ranging from 0.50 to 1.29. At the same wavelength, Metcalf et al.⁶⁹ measured MAC = 0.81 m² g⁻¹ at VOC/NO_x \approx 0.05, which is at a NO_x level substantially higher than typically found in polluted atmospheres (e.g., VOC/NO_x \approx 0.5 to 5⁷⁰). Figure 3a also shows that our MAC values from λ = 300 to 500 nm agree with the results of Updyke et al. within measurement uncertainties. To first order, this suggests that use of high OH concentrations and short reaction times (PAM reactor) gives similar results to the use of low OH concentrations and long reaction times (smog chamber).

Figure 3c shows MAC values measured by Zhong and Jang²³ for SOA from α -pinene photooxidation at 350 and 450 nm in the presence of NO_x (VOC/NO_x = 2.1). Their measurements suggest a MAC at 405 nm \approx 0.015 m² g⁻¹ (O/C ratio not reported). This value is within the range of MAC <0.001 m² g⁻¹ to 0.025 m² g⁻¹ observed in our experiments at 405 nm for O/C ratios ranging from 0.42 to 0.68. These comparisons suggest that under typical ranges of VOC/NO_x, the effect of NO_x on SOA light absorption is small, although under extreme conditions (very high NO_x or low VOC/NO_x), the NO_x may increase absorption substantially.

3.3. Complex Refractive Indices of SOA. Oxidative aging is expected to alter the refractive index of SOA by changing the mean molecular weight, density, and polarizability of the material.^{71,72} Figure 6a and b shows the real (n) and imaginary (k) components of the refractive index at 405 nm (derived from CRD-PAS and SMPS measurements) as a function of the O/C ratio. The n values range from 1.45 (α -pinene SOA at O/C = 0.93) to 1.66 (naphthalene SOA at O/C = 0.55) and are dependent on both the SOA precursor and extent of oxidation (Figure 6a). Corresponding n values obtained at 532 nm range from 1.42 to 1.60 and are systematically lower than values at 405 nm (Figure S3). For each SOA type, the value of n decreases with an increasing O/C ratio. The magnitude of this decrease is precursor-specific, ranging from $\Delta(n)/\Delta(O/C) = -0.055$ (guaiacol SOA) to -0.11 (α -pinene SOA). The absolute n values show a substantial dependence on the nature of the SOA precursor at a specific O/C ratio, with higher values for the aromatic precursors. We note that the decreases in n values with the O/C ratio observed here are opposite in trend to those observed by Cappa et al.⁷² for the heterogeneous OH oxidation of squalane and azelaic acid particles. There can be differences in the chemical reaction pathways and products formed from gas-phase versus condensed phase reactions⁷³

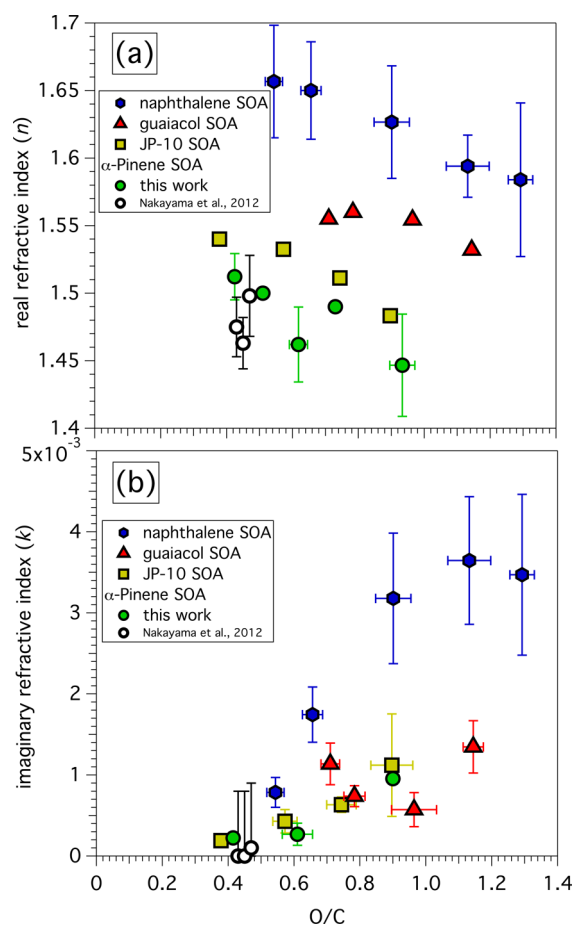


Figure 6. (a) Real and (b) imaginary refractive indices of SOA produced from naphthalene, guaiacol, JP-10, and α -pinene at λ = 405 nm as a function of the O/C ratio. Representative error bars represent $\pm 1\sigma$ in replicate measurements.

which may in part explain differences between the n - O/C relationship observed in this study compared to the heterogeneous oxidation study of Cappa et al.⁷²

Real refractive indices have previously been measured at 405 nm and at 532 nm for α -pinene SOA produced from ozonolysis and from photooxidation across a range of VOC/NO_x ratios. Nakayama et al.²⁵ measured n values of 1.463–1.498 (405 nm) and 1.458–1.476 (532 nm) for O/C ratios ranging from 0.43 to 0.47, and Kim et al.²¹ measured n values of 1.36–1.52 (532 nm), with n increasing in the presence of higher NO_x levels. These values can be compared with our observations, where n ranged from 1.45 (high O/C) to 1.51 (low O/C) at 405 nm and from 1.41 (high O/C) to 1.48 (low O/C) at 532 nm. Figure 6a shows that n values at 405 nm measured in this work and in Nakayama et al.²⁵ are in agreement within uncertainties. Because Kim et al.²¹ do not state O/C ratios or OH exposures, we can only observe that our n values for α -pinene SOA are in the same range.

While the SOA n values at both 405 and 532 nm decrease with the O/C ratio, Figure 6b shows that the imaginary k values at 405 nm typically increase significantly with the O/C ratio, ranging from 1.9×10^{-4} (JP-10 SOA at O/C = 0.47) to 3.6×10^{-3} (naphthalene SOA at O/C = 1.1), consistent with the observed behavior of the MAC discussed above. For JP-10 and α -pinene SOA, k increases monotonically as a function of the O/C ratio. For naphthalene SOA, k initially increases and then

becomes approximately constant above $O/C \approx 0.85$. In contrast, k of guaiacol SOA decreases and then increases with an increasing O/C ratio. The reason for this behavior is, at this point, not evident, although likely related to composition differences between the different SOA types. We also note that the decrease and then increase in k approximately corresponds to an increase and then decrease in the guaiacol SOA H/C ratio (Figure 2). There are very few reported measurements of SOA k values in the literature that can be compared to our results. In one study for SOA formed from OH oxidation of α -pinene in the presence of NO_x , Nakayama et al.²⁵ reported upper-limit k values at 405 nm (8×10^{-3} at $O/C = 0.43$ to 0.47) that are in agreement with our results within uncertainties (Figure 6b). In a similar study, Zhong and Jang²³ reported k values at 350 nm that are constrained only within 2 orders of magnitude (10^{-4} to 10^{-2}).

4. ATMOSPHERIC IMPLICATIONS

The SOA MAC values observed in this study are lower than for OA associated with important sources of primary BrC, such as OA produced by biomass burning (BBOA). At 405 nm, the SOA MAC values ranged from from <0.001 to $0.088 \text{ m}^2 \text{ g}^{-1}$ depending on precursor and oxidation level, compared to MAC ranging from approximately 0.2 to $3 \text{ m}^2 \text{ g}^{-1}$ for BBOA and HULIS (Figure 3). Single scattering albedo (SSA) values at 405 nm ranged from 0.96 to 1.0 for SOA in our measurements (Table S3), compared to $SSA = 0.84$ to 0.93 for BBOA ($\lambda = 450$ to 567 nm).⁷⁴ However, the global production rate of SOA is thought to be significantly larger than the production rate of BBOA. For example, Hallquist et al.¹³ estimated global production rates at 115 TgC yr^{-1} for SOA and 25 TgC yr^{-1} for BBOA. If we estimate a mean MAC $\approx 0.05 \text{ m}^2 \text{ g}^{-1}$ for SOA and $MAC \approx 1 \text{ m}^2 \text{ g}^{-1}$ for BBOA and note that the wavelength dependence of the MAC observed here for SOA is similar to that for BBOA (Figure 3 and Table S2), the positive radiative forcing of SOA is approximately 25% of BBOA on a global scale. While radiative forcing of aerosols depends on many additional factors such their spatial distribution, oxidation level, precursor type, available radiation, and cloud cover, this simple calculation relating global fluxes and MAC of SOA and BBOA provides insight into their relative significance.

Our results can be used as inputs to atmospheric models to refine SOA radiative forcing estimates for specific source regions. Controlled experiments that investigate the influence of NO_x on SOA MAC values and refractive indices over atmospherically relevant VOC/ NO_x ranges will be examined in future studies.

■ ASSOCIATED CONTENT

Supporting Information

Experimental schematic, calculations of time scales for OH oxidation and UV photolysis in the PAM reactor, SOA effective density values, comparison of SOA real refractive index values at 405 and 532 nm, and SOA single scattering albedo values at 405 nm. This material is available free of charge via the Internet at <http://pubs.acs.org>.

■ AUTHOR INFORMATION

Corresponding Author

*E-mail: andrew.lambe@bc.edu.

Notes

The authors declare no competing financial interest.

■ ACKNOWLEDGMENTS

We thank K. Metz (Boston College) for assistance with UV-vis spectrometer operation and M. R. Canagaratna (Aerodyne Research, Inc.) for the use of carboxylic acid standards. This research was supported by the Office of Science (BER), Department of Energy (Atmospheric Science Program) grants No. DE-SC0006980 and DE-FG02-05ER63995, the Environmental Protection Agency grant No. RD-83503301 to Boston College through MIT, and the Atmospheric Chemistry Program of the National Science Foundation grants No. ATM-0854916 and AGS-0904292 to Boston College and Aerodyne Research, Inc., ATM-0837913 to UC Davis, and AGS-0855135 to Pennsylvania State University.

■ REFERENCES

- (1) Andreae, M.; Gelencsér, A. Black carbon or brown carbon? The nature of light-absorbing carbonaceous aerosols. *Atmos. Chem. Phys.* **2006**, *6*, 3131–3148.
- (2) IPCC, The Physical Science Basis. Contribution of Working Group I to the Fourth Assessment Report of the Intergovernmental Panel on Climate Change. 2007.
- (3) Andreae, M. O.; Ramanathan, V. Climate's dark forcings. *Science* **2013**, *340*, 280–281.
- (4) Bond, T.; Bergstrom, R. Light absorption by carbonaceous particles: an investigative review. *Aerosol Sci. Technol.* **2006**, *40*, 27–67.
- (5) Kirchstetter, T. W. Evidence that the spectral dependence of light absorption by aerosols is affected by organic carbon. *J. Geophys. Res.* **2004**, *109*, D21208.
- (6) Pósfai, M. Atmospheric tar balls: particles from biomass and biofuel burning. *J. Geophys. Res.* **2004**, *109*, D06213.
- (7) Chen, Y.; Bond, T. Light absorption by organic carbon from wood combustion. *Atmos. Chem. Phys.* **2010**, *10*, 1773–1787.
- (8) Bahadur, R.; Praveen, P. S.; Xu, Y.; Ramanathan, V. Solar absorption by elemental and brown carbon determined from spectral observations. *Proc. Natl. Acad. Sci.* **2012**, *109*, 17366–17371.
- (9) Lack, D.; Langridge, J.; Bahreini, R.; Cappa, C.; Middlebrook, A.; Schwarz, J. Brown carbon and internal mixing in biomass burning particles. *Proc. Natl. Acad. Sci.* **2012**, *109*, 14802–14807.
- (10) Kirchstetter, T. W.; Thatcher, T. L. Contribution of organic carbon to wood smoke particulate matter absorption of solar radiation. *Atmos. Chem. Phys.* **2012**, *12*, 6067–6072.
- (11) Bond, T. C.; et al. Bounding the role of black carbon in the climate system: a scientific assessment. *J. Geophys. Res.* **2013**, DOI: 10.1002/jgrd.50171.
- (12) Feng, Y.; Ramanathan, V.; Kotamarthi, V. R. Brown carbon: a significant atmospheric absorber of solar radiation? *Atmos. Chem. Phys. Discuss.* **2013**, *13*, 2795–2833.
- (13) Hallquist, M.; Wenger, J.; Baltensperger, U.; Rudich, Y.; Simpson, D.; Claeys, M.; Dommen, J.; Donahue, N.; George, C.; Goldstein, A. The formation, properties and impact of secondary organic aerosol: current and emerging issues. *Atmos. Chem. Phys.* **2009**, *9*, 5155.
- (14) Jacobson, M. Z. Isolating nitrated and aromatic aerosols and nitrated aromatic gases as sources of ultraviolet light absorption. *J. Geophys. Res.* **1999**, *104*, 3527–3542.
- (15) Zhang, X.; Lin, Y.-H.; Surratt, J. D.; Zotter, P.; Prévôt, A. S. H.; Weber, R. J. Light-absorbing soluble organic aerosol in Los Angeles and Atlanta: a contrast in secondary organic aerosol. *Geophys. Res. Lett.* **2011**, *38*, L21810.
- (16) Gelencsér, A.; Hoffer, A.; Kiss, G.; Tombacz, E.; Kurdi, R.; Bencze, L. In-situ formation of light-absorbing organic matter in cloud water. *J. Atmos. Chem.* **2003**, *45*, 25–33.
- (17) Chang, J. L.; Thompson, J. E. Characterization of colored products formed during irradiation of aqueous solutions containing H_2O_2 and phenolic compounds. *Atmos. Environ.* **2010**, *44*, 541–551.
- (18) Ofner, J.; Krüger, H.-U.; Grothe, H.; Schmitt-Kopplin, P.; Whitmore, K.; Zetzsch, C. Physico-chemical characterization of SOA

derived from catechol and guaiacol – a model substance for the aromatic fraction of atmospheric HULIS. *Atmos. Chem. Phys.* **2011**, *11*, 1–15.

(19) Nakayama, T.; Matsumi, Y.; Sato, K.; Imamura, T.; Yamazaki, A.; Uchiyama, A. Laboratory studies on optical properties of secondary organic aerosols generated during the photooxidation of toluene and the ozonolysis of α -pinene. *J. Geophys. Res.* **2010**, *115*, D24204.

(20) Nakayama, T.; Sato, K.; Matsumi, Y.; Imamura, T.; Yamazaki, A.; Uchiyama, A. Wavelength and NO_x dependent complex refractive index of SOAs generated from the photooxidation of toluene. *Atmos. Chem. Phys.* **2013**, *13*, 531–545.

(21) Kim, H.; Barkey, B.; Paulson, S. Real refractive indices and formation yields of secondary organic aerosol generated from photooxidation of limonene and α -pinene: the effect of the HC/ NO_x ratio. *J. Phys. Chem. A* **2012**, *116*, 6059–6067.

(22) Kim, H.; Paulson, S. E. Real refractive indices and volatility of secondary organic aerosol generated from photooxidation and ozonolysis of limonene, α -pinene and toluene. *Atmos. Chem. Phys. Discuss.* **2013**, *13*, 1949–1977.

(23) Zhong, M.; Jang, M. Light absorption coefficient measurement of SOA using a UV-visible spectrometer connected with an integrating sphere. *Atmos. Environ.* **2011**, *45*, 4263–4271.

(24) Zhong, M.; Jang, M.; Oliferenko, A.; Pillai, G. G.; Katritzky, A. R. The SOA formation model combined with semiempirical quantum chemistry for predicting UV-vis absorption of secondary organic aerosols. *Phys. Chem. Chem. Phys.* **2012**, *14*, 9058–9066.

(25) Nakayama, T.; Sato, K.; Matsumi, Y.; Imamura, T.; Yamazaki, A.; Uchiyama, A. Wavelength dependence of refractive index of secondary organic aerosols generated during the ozonolysis and photooxidation of α -pinene. *SOLA* **2012**, *8*, 119–123.

(26) Updyke, K. M.; Nguyen, T. B.; Nizkorodov, S. A. Formation of brown carbon via reactions of ammonia with secondary organic aerosols from biogenic and anthropogenic precursors. *Atmos. Environ.* **2012**, *63*, 22–31.

(27) Bones, D. L.; Henricksen, D. K.; Mang, S. A.; Gonsior, M.; Bateman, A. P.; Nguyen, T. B.; Cooper, W. J.; Nizkorodov, S. A. Appearance of strong absorbers and fluorophores in limonene- O_3 secondary organic aerosol due to NH_4^+ -mediated chemical aging over long time scales. *J. Geophys. Res.* **2010**, *115*, D05203.

(28) Yu, G.; Bayer, A.; Galloway, M.; Korshavn, K.; Fry, C.; Keutsch, F. Glyoxal in aqueous ammonium sulfate solutions: products, kinetics and hydration effects. *Environ. Sci. Technol.* **2011**, *45*, 6336–6342.

(29) Nguyen, T. B.; Lee, P. B.; Updyke, K. M.; Bones, D. L.; Laskin, J.; Laskin, A.; Nizkorodov, S. A. Formation of nitrogen- and sulfur-containing light-absorbing compounds accelerated by evaporation of water from secondary organic aerosols. *J. Geophys. Res.* **2012**, *117*, D01207.

(30) Ng, N. L.; et al. Organic aerosol components observed in Northern Hemispheric datasets from Aerosol Mass Spectrometry. *Atmos. Chem. Phys.* **2010**, *10*, 4625–4641.

(31) Spracklen, D. V.; Jimenez, J. L.; Carslaw, K. S.; Worsnop, D. R.; Evans, M. J.; Mann, G. W.; Zhang, Q.; Canagaratna, M. R.; Allan, J.; Coe, H.; McFiggans, G.; Rap, A.; Forster, P. Aerosol mass spectrometer constraint on the global secondary organic aerosol budget. *Atmos. Chem. Phys.* **2011**, *11*, 12109–12136.

(32) Bateman, A. P.; Nizkorodov, S. A.; Laskin, J.; Laskin, A. Photolytic processing of secondary organic aerosols dissolved in cloud droplets. *Phys. Chem. Chem. Phys.* **2011**, *13*, 12199.

(33) Kang, E.; Root, M.; Brune, W. Introducing the concept of Potential Aerosol Mass (PAM). *Atmos. Chem. Phys.* **2007**, *7*, 5727–5744.

(34) Dinar, E.; Mentel, T.; Rudich, Y. The density of humic acids and humic like substances (HULIS) from fresh and aged wood burning and pollution aerosol particles. *Atmos. Chem. Phys.* **2006**, *6*, 5213–5224.

(35) Lambe, A. T.; Ahern, A. T.; Williams, L. R.; Slowik, J. G.; Wong, J. P. S.; Abbatt, J. P. D.; Brune, W. H.; Ng, N. L.; Wright, J. P.; Croasdale, D. R.; Worsnop, D. R.; Davidovits, P.; Onasch, T. B. Characterization of aerosol photooxidation flow reactors: heteroge-

neous oxidation, secondary organic aerosol formation and cloud condensation nuclei activity measurements. *Atmos. Meas. Tech.* **2011**, *4*, 445–461.

(36) Mao, J.; Ren, X.; Brune, W.; Olson, J.; Crawford, J.; Fried, A.; Huey, L.; Cohen, R.; Heikes, B.; Singh, H. Airborne measurement of OH reactivity during INTEX-B. *Atmos. Chem. Phys.* **2009**, *9*, 163–173.

(37) Drewnick, F.; Hings, S. S.; Decarlo, P. F.; Jayne, J. T.; Gonin, M.; Fuhrer, K.; Weimer, S.; Jimenez, J. L.; Demerjian, K. L.; Borrmann, S.; Worsnop, D. R. A new time-of-flight aerosol mass spectrometer (TOF-AMS)-instrument description and first field deployment. *Aerosol Sci. Technol.* **2005**, *39*, 637–658.

(38) Sueper, D. ToF-AMS Analysis Software, 2010. Available at <http://cires.colorado.edu/jimenez-group/ToFAMSResources/ToFSoftware/index.html> (accessed May 19, 2013).

(39) Aiken, A.; DeCarlo, P.; Kroll, J.; Worsnop, D.; Huffman, J.; Docherty, K.; Ulbrich, I.; Mohr, C.; Kimmel, J.; Sueper, D. O/C and OM/OC ratios of primary, secondary, and ambient organic aerosols with high-resolution time-of-flight aerosol mass spectrometry. *Environ. Sci. Technol.* **2008**, *42*, 4478–4485.

(40) Baduel, C.; Voisin, D.; Jaffrezo, J. Comparison of analytical methods for HULIS measurements in atmospheric particles. *Atmos. Chem. Phys.* **2009**, *9*, 5949–5962.

(41) Lack, D. A.; Lovejoy, E. R.; Baynard, T.; Pettersson, A.; Ravishankara, A. R. Aerosol absorption measurement using photoacoustic spectroscopy: sensitivity, calibration, and uncertainty developments. *Aerosol Sci. Technol.* **2006**, *40*, 697–708.

(42) Baynard, T.; Lovejoy, E. R.; Pettersson, A.; Brown, S. S.; Lack, D.; Osthoff, H.; Massoli, P.; Ciciora, S.; Dube, W. P.; Ravishankara, A. R. Design and application of a pulsed cavity ring-down aerosol extinction spectrometer for field measurements. *Aerosol Sci. Technol.* **2007**, *41*, 447–462.

(43) Langridge, J. M.; Richardson, M. S.; Lack, D.; Law, D.; Murphy, D. M. Aircraft instrument for comprehensive characterization of aerosol optical properties, Part I: wavelength-dependent optical extinction and its relative humidity dependence measured using cavity ringdown spectroscopy. *Aerosol Sci. Technol.* **2011**, *45*, 1305–1318.

(44) Lack, D. A.; Richardson, M. S.; Law, D.; Langridge, J. M.; Cappa, C. D.; McLaughlin, R. J.; Murphy, D. M. Aircraft instrument for comprehensive characterization of aerosol optical properties, Part 2: black and brown carbon absorption and absorption enhancement measured with photo acoustic spectroscopy. *Aerosol Sci. Technol.* **2012**, *46*, 555–568.

(45) Cappa, C. D.; et al. Radiative absorption enhancements due to the mixing state of atmospheric black carbon. *Science* **2012**, *337*, 1078–1081.

(46) DeCarlo, P.; Slowik, J.; Worsnop, D.; Davidovits, P.; Jimenez, J. Particle morphology and density characterization by combined mobility and aerodynamic diameter measurements. Part 1: theory. *Aerosol Sci. Technol.* **2004**, *38*, 1185–1205.

(47) Bohren, C. F.; Huffman, D. R. *Absorption and Scattering of Light by Small Particles*; Wiley-Interscience: New York, 1998.

(48) van Krevelen, D. Graphical-statistical method for the study of structure and reaction processes of coal. *Fuel* **1950**, *24*, 269–284.

(49) Kwok, E.; Atkinson, R. Estimation of hydroxyl radical reaction rate constants for gas-phase organic compounds using a structure-reactivity relationship: an update. *Atmos. Environ.* **1995**, *29*, 1685–1695.

(50) Yee, L. D.; Kautzman, K. E.; Loza, C. L.; Schilling, K. A.; Coggon, M. M.; Chhabra, P. S.; Chan, M. N.; Chan, A. W. H.; Hersey, S. P.; Crounse, J. D.; Wennberg, P. O.; Flagan, R. C.; Seinfeld, J. H. Secondary organic aerosol formation from biomass burning intermediates: phenol and methoxyphenols. *Atmos. Chem. Phys. Discuss.* **2013**, *13*, 3485–3532.

(51) Heald, C. L.; Kroll, J. H.; Jimenez, J. L.; Docherty, K. S.; Decarlo, P. F.; Aiken, A. C.; Chen, Q.; Martin, S. T.; Farmer, D. K.; Artaxo, P. A simplified description of the evolution of organic aerosol composition in the atmosphere. *Geophys. Res. Lett.* **2010**, *37*, L08803.

(52) Lambe, A. T.; Onasch, T. B.; Croasdale, D. R.; Wright, J. P.; Martin, A. T.; Franklin, J. P.; Massoli, P.; Kroll, J. H.; Canagaratna, M.

R.; Brune, W. H.; Worsnop, D. R.; Davidovits, P. Transitions from functionalization to fragmentation reactions of laboratory secondary organic aerosol (SOA) generated from the OH oxidation of alkane precursors. *Environ. Sci. Technol.* **2012**, *46*, 5430–5437.

(53) Hoffer, A.; Gelencsér, A.; Guyon, P.; Kiss, G.; Schmid, O.; Frank, G.; Artaxo, P.; Andreae, M. Optical properties of humic-like substances (HULIS) in biomass-burning aerosols. *Atmos. Chem. Phys.* **2006**, *6*, 3563–3570.

(54) Clarke, A.; McNaughton, C.; Kapustin, V.; Shinozuka, Y.; Howell, S.; Dibb, J.; Zhou, J.; Anderson, B.; Brekhovskikh, V.; Turner, H.; Pinkerton, M. Biomass burning and pollution aerosol over North America: organic components and their influence on spectral optical properties and humidification response. *J. Geophys. Res.* **2007**, *112*.

(55) Alexander, D. T. L.; Crozier, P. A.; Anderson, J. R. Brown carbon spheres in East Asian outflow and their optical properties. *Science* **2008**, *321*, 833–836.

(56) Chakrabarty, R. K.; Moosmüller, H.; Chen, L.-W. A.; Lewis, K.; Arnott, W. P.; Mazzoleni, C.; Dubey, M. K.; Wold, C. E.; Hao, W. M.; Kreidenweis, S. M. Brown carbon in tar balls from smoldering biomass combustion. *Atmos. Chem. Phys.* **2010**, *10*, 6363–6370.

(57) Emery, K. ASTM G0173-03 reference solar spectral irradiance: Air Mass 1.5, 2009. Available at <http://rredc.nrel.gov/solar/spectra/am1.5/#about> (accessed May 19, 2013).

(58) Yee, L. D.; Craven, J. S.; Loza, C. L.; Schilling, K. A.; Ng, N. L.; Canagaratna, M. R.; Ziemann, P. J.; Flagan, R. C.; Seinfeld, J. H. Secondary organic aerosol formation from low-NO_x photooxidation of dodecane: evolution of multigeneration gas-phase chemistry and aerosol composition. *J. Phys. Chem. A* **2012**, *116*, 6211–6230.

(59) Eddingsaas, N. C.; Loza, C. L.; Yee, L. D.; Seinfeld, J. H.; Wennberg, P. O. α -Pinene photooxidation under controlled chemical conditions - Part 1: gas-phase composition in low- and high-NO_x environments. *Atmos. Chem. Phys.* **2012**, *12*, 6489–6504.

(60) Eddingsaas, N. C.; Loza, C. L.; Yee, L. D.; Chan, M.; Schilling, K. A.; Chhabra, P. S.; Seinfeld, J. H.; Wennberg, P. O. α -Pinene photooxidation under controlled chemical conditions - Part 2: SOA yield and composition in low- and high-NO_x environments. *Atmos. Chem. Phys.* **2012**, *12*, 7413–7427.

(61) Walser, M.; Park, J.; Gomez, A.; Russell, A.; Nizkorodov, S. Photochemical aging of secondary organic aerosol particles generated from the oxidation of d-limonene. *J. Phys. Chem. A* **2007**, *111*, 1907–1913.

(62) Pan, X.; Underwood, J.; Xing, J.; Mang, S.; Nizkorodov, S. Photodegradation of secondary organic aerosol generated from limonene oxidation by ozone studied with chemical ionization mass spectrometry. *Atmos. Chem. Phys.* **2009**, *9*, 3851–3865.

(63) Craven, J. S.; Yee, L. D.; Ng, N. L.; Canagaratna, M. R.; Loza, C. L.; Schilling, K. A.; Yatavelli, R. L. N.; Thornton, J. A.; Ziemann, P. J.; Flagan, R. C.; Seinfeld, J. H. Analysis of secondary organic aerosol formation and aging using positive matrix factorization of high-resolution aerosol mass spectra: application to the dodecane low-NO_x system. *Atmos. Chem. Phys.* **2012**, *12*, 11795–11817.

(64) Sato, K.; Takami, A.; Kato, Y.; Seta, T.; Fujitani, Y.; Hikida, T.; Shimono, A.; Imamura, T. AMS and LC/MS analyses of SOA from the photooxidation of benzene and 1,3,5-trimethylbenzene in the presence of NO_x: effects of chemical structure on SOA aging. *Atmos. Chem. Phys.* **2012**, *12*, 4667–4682.

(65) Gratien, A.; Johnson, S.; Ezell, M.; Dawson, M.; Bennett, R.; Finlayson-Pitts, B. Surprising formation of *p*-cymene in the oxidation of α -pinene in air by the atmospheric oxidants OH, O₃, and NO₃. *Environ. Sci. Technol.* **2011**, *45*, 2755–2760.

(66) Kautzman, K.; Surratt, J.; Chan, M.; Chan, A.; Hersey, S.; Chhabra, P.; Dalleska, N.; Wennberg, P.; Flagan, R.; Seinfeld, J. Chemical composition of gas-and aerosol-phase products from the photooxidation of naphthalene. *J. Phys. Chem. A* **2010**, *114*, 913–934.

(67) Ritchie, J.; Perdue, E. Proton-binding study of standard and reference fulvic acids, humic acids, and natural organic matter. *Geochim. Cosmochim. Acta* **2003**, *67*, 85–96.

(68) Baigorri, R.; Fuentes, M.; González-Gaitano, G.; García-Mina, J.; Almendros, G.; González-Vila, F. Complementary multianalytical

approach to study the distinctive structural features of the main humic fractions in solution: gray humic acid, brown humic acid, and fulvic acid. *J. Agric. Food Chem.* **2009**, *57*, 3266–3272.

(69) Metcalf, A. R.; Loza, C. L.; Coggon, M. M.; Craven, J. S.; Jonsson, H. H.; Flagan, R. C.; Seinfeld, J. H. Secondary organic aerosol coating formation and evaporation: chamber studies using black carbon seed aerosol and the single-particle soot photometer. *Aerosol Sci. Technol.* **2013**, *47*, 326–347.

(70) Finlayson-Pitts, B. J.; Pitts, J. N., Jr. *Chemistry of the Upper and Lower Atmosphere: Theory, Experiments, and Applications*; Academic Press: San Diego, 2000.

(71) Liu, Y.; Daum, P. H. Relationship of refractive index to mass density and self-consistency of mixing rules for multicomponent mixtures like ambient aerosols. *J. Aerosol Sci.* **2008**, *39*, 974–986.

(72) Cappa, C. D.; Che, D. L.; Kessler, S. H.; Kroll, J. H.; Wilson, K. R. Variations in organic aerosol optical and hygroscopic properties upon heterogeneous OH oxidation. *J. Geophys. Res.* **2011**, *116*, D15204.

(73) Hearn, J. D.; Renbaum, L. H.; Wang, X.; Smith, G. D. Kinetics and products from reaction of Cl radicals with dioctyl sebacate (DOS) particles in O₂: A model for radical-initiated oxidation of organic aerosols. *Phys. Chem. Chem. Phys.* **2007**, *9*, 4803.

(74) Reid, J. S.; Eck, T. F.; Christopher, S. A.; Koppmann, R.; Dubovik, O.; Eleuterio, D. P.; Holben, B. N.; Reid, E. A.; Zhang, J. A review of biomass burning emissions Part III: intensive optical properties of biomass burning particles. *Atmos. Chem. Phys.* **2005**, *5*, 827–849.